JOURNAL OF APPLIED ELECTROCHEMISTRY **24** (1994) 107–113

Oxidation of iodide to iodate concurrently with evolution of oxygen at Kelgraf composite electrodes

J. E. VITT

Department of Chemistry, University of South Dakota, Vermillion, SD 57069, USA

D. C. JOHNSON

Department of Chemistry and Ames Laboratory, Iowa State University, Ames, IA 50011, USA

Received 14 June 1993; revised 19 July 1993

The oxidation of I^- to IO_3^- in acidic media occurs at numerous electrode materials at potential values corresponding to the anodic discharge of H_2O with simultaneous evolution of oxygen. In the study reported here the anodic current density for IO_3^- production was measured by difference voltammetry at rotated disc electrodes (r.d.e.'s) constucted from pure glassy carbon (GC) and Kelgraf (graphite plus Kel-F) composite materials. These signal values (S) were normalized relative to the background current (B) for oxygen evolution measured at 1.75 V vs SCE, a potential corresponding to the transport-limited production of IO_3^- at GC. Despite a small positive shift in $E_{1/2}$ with decreasing fractional active area, the signal-to-background ratio (S/B) at the Kelgraf electrodes was enhanced relative to that for the GC electrode. For example, S/B at a 2% Kelgraf r.d.e. was nine times larger than at a GC r.d.e. This corresponds to an increase in current efficiency ($S/(S+B)$) for IO_3^- production from about 50% at the GC r.d.e. to about 90% at 2% Kelgraf r.d.e. This is explained on the basis of (i) a significant decrease in total background current as a result of the decreased fraction of the Kelgraf surface that corresponds to carbon, and (ii) a larger flux density of I^- at the carbon microelectrodes in the Kelgraf r.d.e., as compared to the GC r.d.e., as a result of radial diffusion, i.e. the so-called 'edge effect'.

1. Introduction

Anodic discharge of H_2O with production of adsorbed hydroxyl radicals, as shown in Equation 1, is the initial step in the mechanism for anodic evolution of oxygen, as shown in Equation 2 [1–4]. This production of $\cdot OH_{ads}$ is also believed to be a requisite step in anodic O-transfer reactions, as illustrated by Equation 3 where R and RO represent the reactant and product, respectively [5–11].

$$H_2O \longrightarrow \cdot OH_{ads} + H^+ + e^- \quad (1)$$

$$H_2O + \cdot OH_{ads} \longrightarrow O_2 + 3H^+ + 3e^- \quad (2)$$

$$R + \cdot OH_{ads} \longrightarrow RO + H^+ + e^- \quad (3)$$

Evidence supporting this conclusion was obtained in our laboratory for oxidation of I^- to IO_3^- at Pt, Au, Pd, Ir, and GC [5]. In that study, a linear correlation was determined to exist between the $E_{1/2}$ values for oxidation of I^- to IO_3^- and the oxygen-evolution overpotential at the various anode materials. Conversely, $E_{1/2}$ values for oxidation of I^- to I_2 were determined to be independent of the oxygen-evolution overpotential, as is expected for reactions that do not involve an O-transfer mechanism.

As a result of the mechanistic link between O-transfer and oxygen-evolution reactions, the anodic signal of interest (S) for O-transfer reactions can be obscured by a large background current (B) resulting from the simultaneous evolution of oxygen. The consequence of a large background current can include low values of the signal-to-background ratio (S/B) in electroanalytical applications and low current efficiencies ($S/(S+B)$) in industrial electrolytic processes. For electroanalytical applications of anodic O-transfer reactions at hydrodynamic electrodes, the transport-dependent current of interest (S) can be extracted from the total observed current ($S+B$) using hydrodynamically modulated voltammetry [6, 7] or difference voltammetry [5]. However, this approach is not useful for improving $S/(S+B)$ in industrial applications of O-transfer reactions.

It is the premise of research reported here that the goal of high current efficiency in anodic O-transfer reactions can be achieved for composite electrode materials when catalyst particles are uniformly distributed as microelectrode arrays within the inert surfaces. It is well established that S/B can be significantly larger at microelectrodes and microelectrode arrays, as compared to conventional macro-sized electrodes [12, 13]. This has been demonstrated for microelectrode arrays fabricated from graphite and Kel-F (poly(chlorotrifluoroethylene)), commonly called 'Kelgraf electrodes', and applied for voltammetric and chronoamperometric measurements in stationary solutions [14–17],

0021-891X

and amperometric detection in flow-through cells [14, 18–23]. Recently, large increases (>10 times) in current density were reported for Kelgraf and Au/Kelgraf rotated disc electrodes (r.d.e.'s) in comparison to solid GC and Au r.d.e.'s [24].

Here, we report that values of S/B for oxidation of I^- to IO_3^- simultaneously with oxygen evolution at Kelgraf electrodes are increased as the fractional active area is decreased. These results support the premise that current efficiencies for electrolytic processes can be larger at microelectrode arrays as compared to pure electrodes under conditions of large applied potentials that result in anodic or cathodic discharge of solvent.

2. Experimental details

2.1. *Equipment*

The electrochemical instrumentation has already been described [24]. Scanning electron micrographs were obtained by measuring the backscattered electron signal with a JSM 840A scanning microscope (JEOL) after evaporation of carbon films (Edwards) on the Kelgraf electrodes. Kelgraf disc electrodes with a geometric area of 1.33 cm^2 were fabricated according to a published procedure [16, 24], with the exception that the composite mixtures were compressed at about 20 000 lb in^{-2} (~140 MPa). All electrodes had a negligible resistance (<10 Ω) except for the 2% Kelgraf electrode (150 Ω). The GC r.d.e. (0.196 cm^2) was from Pine Instrument Co. All potential values are reported with reference to the saturated calomel electrode (SCE).

2.2. *Reagents*

Potassium iodide was reagent grade (Fisher Scientific). Deionized water was prepared by passage through two D-45 deionizing tanks (Culligan), followed by purification in a Milli-Q system (Millipore).

2.3. *Procedures*

Electrodes were polished successively with 1 μm, 0.3 μm, and 0.05 μm alumina in H_2O on Nylon (Buehler Ltd). Current–potential (i–E) curves were recorded after cycling the electrode potential between −0.3 and 1.75 V for about 10 min in 0.1 M H_2SO_4.

Residual i–E curves were recorded immediately prior to the addition of KI. Tafel data, i.e. plots of $\ln\{i\}$ against $(E - E^{0\prime})$, were analysed according to Equation 4 for anodic evolution of oxygen during the negative potential scan over the range 1.75 to 1.65 V.

$$\ln i = \ln i_0 - \frac{\alpha n F(E - E^{0\prime})}{RT} \qquad (4)$$

In Equation 4, α is the transfer coefficient, $E^{0\prime}$ is the thermodynamic potential for the oxidation of H_2O to O_2 at pH 1.0 (0.93 V vs SCE), and the remaining terms have their usual electrochemical significance.

Values of electrode current at the r.d.e.'s were compared to the transport-limited value (i_{lim}) predicted by the Levich equation (Equation 5) at uniformly active r.d.e.'s [25].

$$i_{lim} = \frac{0.554}{0.8934 + 0.316(D/\nu)^{0.36}} nFA_{geo}D^{2/3}\nu^{-1/6}\omega^{1/2}C^b \qquad (5)$$

In Equation 5, A_{geo} is the geometric area of the disc electrode (cm^2), D is the diffusion coefficient (2.045×10^{-5} cm^2 s^{-1} for I^-) [26], ν is the kinematic viscosity (~ 0.01 cm^2 s^{-1}), ω is the rotation velocity (rad s^{-1}), and C^b is the bulk concentration of electroactive species (mol cm^{-3}).

Difference voltammetric curves were calculated by subtraction of voltammetric data (i–E) obtained for changes in C^b at a single value of $\omega^{1/2}$, designated as $\Delta i\{\Delta C^b\}$–E curves; and for changes in $\omega^{1/2}$ at a single value of C^b, designated as $\Delta i\{\Delta\omega^{1/2}\}$–$E$ curves. Combinations of values for C^b and $\omega^{1/2}$ were: $C^b = 0.50$ and 1.00 mM ($\Delta C^b = 0.50$ mM) for $\omega^{1/2} = 6.47\ s^{-1/2}$; and $\omega^{1/2} = 6.47$ and $12.95\ s^{-1/2}$ ($\Delta\omega^{1/2} = 6.47\ s^{-1/2}$) for $C^b = 0.50$ mM. These pairs were chosen so that values of $\Delta i\{\Delta C^b\}$ and $\Delta i\{\Delta\omega^{1/2}\}$ measured for transport-limited processes at uniformly-active electrodes (solid GC) will equal i_{lim} values calculated by Equation 5 for $C^b = 0.5$ mM at $\omega^{1/2} = 6.47\ s^{-1/2}$. For electrodes with non-uniformly accessible surfaces (Kelgraf), $\Delta i\{\Delta\omega^{1/2}\}$ and $\Delta i\{\Delta C^b\}$ are expected not to be equal and, furthermore, these experimental values cannot be predicted on the basis of Equation 5. In the case where Kelgraf electrodes might approximate ideal microarray electrodes, the electrode current is predicted to be independent of rotational velocity, i.e. $\Delta i\{\Delta\omega^{1/2}\} = 0$.

3. Results and discussion

3.1. *Voltammetric response at the GC electrode*

The voltammetric response of I^- at the solid GC r.d.e. was considered to be representative of that for a solid graphite electrode. This conclusion is supported by the observations of identical $E_{1/2}$ values for oxidation of I^- to I_2 and nearly identical $E_{1/2}$ values for oxidation of I^- to IO_3^- at the GC and 25% Kelgraf electrodes. Furthermore, values of the oxygen-evolution overpotential were virtually identical when measured at the same current density for the various electrodes.

The residual i–E response for the GC r.d.e. in 0.1 M H_2SO_4 is shown in Fig. 1 (curve a). Rigorous evolution of oxygen occurs at $E >\sim 1.5$ V, corresponding to the sharp increase in background current. The value of 1.75 V was chosen for the positive scan limit in voltammetric experiments and for measurements of the oxygen-evolution background current. The voltammetric response in the presence of 0.50 mM I^- is also shown in Fig. 1 (curve b). Three anodic waves

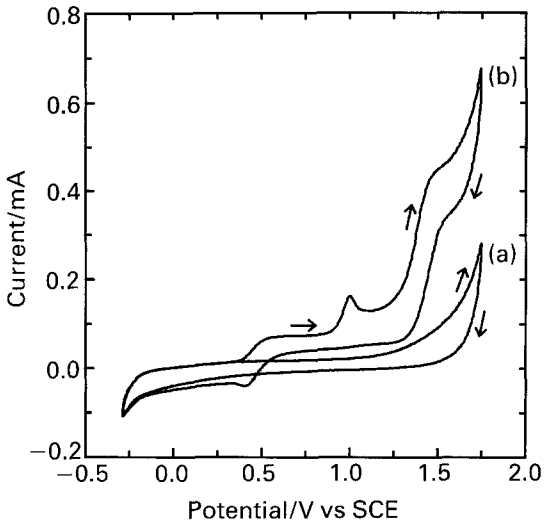

Fig. 1. Voltammetric response (i–E) for I^- at a solid GC r.d.e. in 0.1 M H_2SO_4 at a scan rate of 100 mV s^{-1}. Rotational velocity: (a) 167.6 and (b) 41.9 s^{-1}. Conc. I^-: (a) 0 and (b) 0.50 mM.

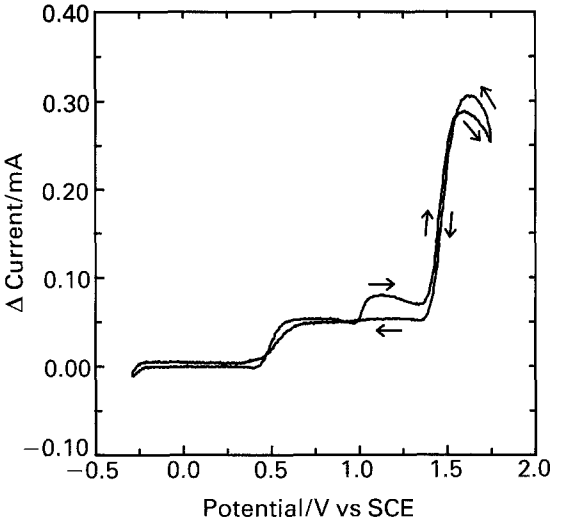

Fig. 2. Difference voltammetric response ($\Delta i\{\Delta\omega^{1/2}\}$–$E$) calculated from i–E curves obtained for 0.5 mM I^- at a solid GC r.d.e. in 0.1 M H_2SO_4 for rotational velocities of 167.6 and 41.9 s^{-1}, i.e. $\Delta\omega^{1/2} = 6.47\ s^{-1/2}$, and a scan rate of 100 mV s^{-1}.

are evident. The first wave ($E_{1/2} = 0.46$ V) corresponds to oxidation of I^- to I_2 which occurs at a transport-limited rate in the region about 0.55–0.85 V. The second wave, observed during the positive scan in the region 0.95–1.25 V, is tentatively concluded to correspond to the oxidation of I^- to IO^- by a two-electron process [5]. Of primary interest in this study is the third wave ($E_{1/2} = 1.36$ V) which is concluded to correspond to the oxidation of I^- to IO_3^- ($E^{0\prime} = 0.785$ V) [27]. In this same potential region, the evolution of oxygen contributes significantly to the total current, leading to poor voltammetric resolution of the two faradaic processes and the absence of a significant current plateau representing the transport-limited oxidation of I^- to IO_3^-. Furthermore, the presence of I^- causes a small positive shift of the oxygen-evolution overpotential. Therefore, it is not possible to calculate the net i–E response for IO_3^- production by subtraction of the residual response measured in the absence of I^- from the total response in the presence of I^-. In this study, the net response for IO_3^- production was calculated by subtraction of voltammetric data obtained for differing values of rotational velocity and I^- concentration.

A plot of $\Delta i\{\Delta\omega^{1/2}\}$ against E is shown in Fig. 2 for $\Delta\omega^{1/2} = 6.47\ s^{-1/2}$ and $C^b = 0.50$ mM. As discussed previously for Fig. 1 (curve b), three anodic waves are observed for the positive scan. The plateau value of $\Delta i\{\Delta\omega^{1/2}\}$ for I_2 production (0.053 mA at about 0.75 V) is 90% of the value 0.059 mA calculated by Equation 5 ($n = 1$ eq mol^{-1}). The small difference between the observed and theoretical values is attributed to the cumulative effect of errors in the values for C^b, A, D and ν used in Equation 5. Whereas $\Delta i\{\Delta\omega^{1/2}\}$ is expected to represent only the transport-dependent components of the total electrode current, a limiting current plateau is not observed in Fig. 2 for IO_3^- production ($E_{1/2} = 1.45$ V). The maximum value of $\Delta i\{\Delta\omega^{1/2}\}$ for IO_3^- production (0.31 mA at 1.65 V) is 86% of the theoretical value (0.35 mA for $n = 6$ eq mol^{-1}). This agreement between observation and prediction is virtually identical to that for I_2 production and we conclude that $\Delta i\{\Delta\omega^{1/2}\}$ for IO_3^- production at 1.65 V is virtually the transport-limited value. The maximum value of $\Delta i\{\Delta\omega^{1/2}\}$ in Fig. 2 for the presumed production of IO^- (0.081 mA at 1.1 V) is only 69% of the predicted value (0.118 mA for $n = 2$ eq mol^{-1}). We interpret this result to indicate that oxidation of I^- to IO^- is characterized by slow heterogeneous kinetics and, therefore, $\Delta i\{\Delta\omega^{1/2}\}$ cannot be predicted accurately on the basis of Equation 5 for transport-limited processes.

A plot of $\Delta i\{\Delta C^b\}$ against E is shown in Fig. 3 for $\Delta C^b = 0.50$ mM and $\omega^{1/2} = 6.47\ s^{-1/2}$. As stipulated in the experimental section, pairs of values of $\omega^{1/2}$ and C^b were chosen so that $\Delta i\{\Delta C^b\}$–E and $\Delta i\{\Delta\omega^{1/2}\}$–$E$ curves will be equivalent for voltammetric processes under mass-transport control. The limiting values of $\Delta i\{\Delta C^b\}$ in Fig. 3 for production of iodine (0.055 mA at ~0.75 V) and IO_3^- (0.306 mA

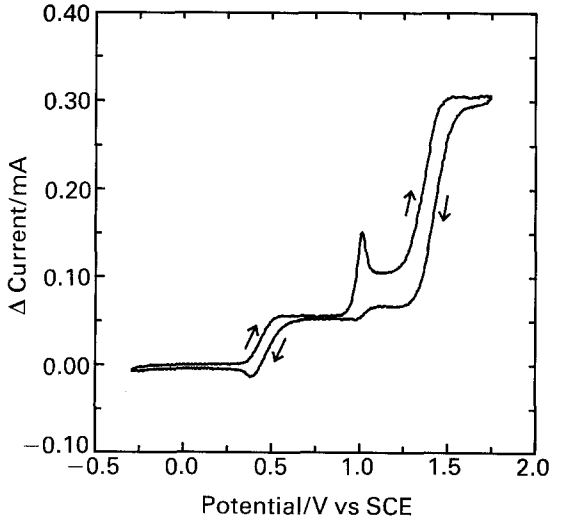

Fig. 3. Difference voltammetric response ($\Delta i\{\Delta C^b\}$–E) calculated from i–E curves obtained for 1.0 and 0.5 mM I^-, i.e. $\Delta C^b = 0.50$ mM, at a solid GC r.d.e. in 0.1 M H_2SO_4 using a rotational velocity of 41.9 rad s^{-1}, and a scan rate of 100 mV s^{-1}.

at ~1.6 V) are virtually identical to the corresponding values in Fig. 2. However, the wave for IO_3^- production in Fig. 3 appears better resolved from the background current than in Fig. 2 and a clear plateau response is observed in the region about 1.5–1.75 V. Values of $\Delta i\{\Delta C^b\}$ for IO^- production in Fig. 3 are significantly larger than in Fig. 2. Furthermore, for the positive scan in the region about 1.1–1.3 V, the response for IO^- production is consistent with a transport-limited oxidation of I^- ($n = 2$ eq mol^{-1}). The smaller response to change of $\omega^{1/2}$ (Fig. 2), as compared to change of C^b (Fig. 3), is consistent with the designation of slow heterogeneous kinetics for this anodic mechanism. It is significant that a peak is observed during the positive scan at about 1.0 V in Fig. 3 but not in Fig. 2. We speculate this peak corresponds to oxidation of adsorbed iodine because the signal responds to changes in C^b but not $\omega^{1/2}$.

3.2. *Scanning electron microscopy*

Micrographs of 3% and 25% Kelgraf electrodes are shown in Figs 4 and 5, respectively. The black regions are graphite and the grey regions are Kel-F, as verified by energy dispersive X-ray analysis [24]. It is apparent that these Kelgraf electrodes are composed of graphitic microelectrodes of widely varying size and geometry surrounded by large insulating regions of Kel-F. Evidently, during fabrication, the graphite particles fill the interstices between the larger Kel-F particles. Hence, the dimensions of the active graphitic regions are dependent on both the amount of graphite used and the size and shape of the Kel-F particles. For example, the 3% Kelgraf electrode (Fig. 4) consists of thin (<10 μm wide) graphitic regions that are interconnected to give an appearance similar to a spider's web. Conversely, the 25% Kelgraf electrode (Fig. 5) has graphitic regions that are nearly as wide as they are long and that are interconnected by narrow graphitic regions similar to those seen in the 3% Kelgraf electrode.

Because of the extreme irregularity in size, shape, and separation of the active graphitic regions in Kelgraf electrodes, an exact analytical solution has not been obtained for the expected current density under various voltammetric conditions. However, it is well established that larger current densities can be achieved by increasing the perimeter-to-area ratio

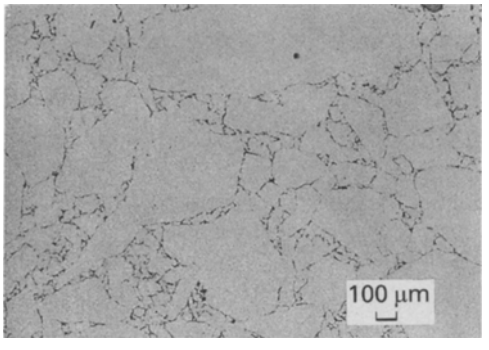

Fig. 4. Micrograph of 3% Kelgraf electrode.

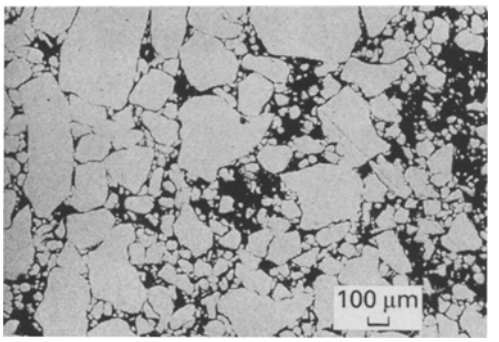

Fig. 5. Micrograph of 25% Kelgraf electrode.

of the active regions. This is a beneficial consequence of higher rates of mass transport to the edges of the inlaid microelectrodes, i.e. the so-called 'edge effect' [12, 13]. Thus, for a constant fractional active area, the current density increases as the active sites are made smaller and more numerous [17, 23]. Therefore, on the basis of Figs 4 and 5, S/B for the 3% Kelgraf electrode is expected to be larger than that for the 25% Kelgraf electrode.

The fractions of geometric areas corresponding to graphite were estimated from SEM data for the Kelgraf electrodes. The values are listed here together with the nominal fractional area (in parenthesis) estimated from the composition: 1.5% (2%), 2.5% (3%), 9.0% (10%), and 18.3% (25%). These values represent averages of SEM measurements for six different regions of one electrode for each composition, with the exception that the value for 10% Kelgraf is based on four measurements. The fractional graphitic areas estimated from SEM data consistently are lower than the nominal values estimated from the composition. This probably results from mechanical loss of some graphite particles during polishing. Micrographs for 25% Kelgraf electrodes taken at high magnification revealed extensive pitting within the interior of the graphitic regions where the absence of Kel-F binder results in mechanical instability. Pitting was not as apparent at lower fractional graphite content.

3.3. *Voltammetric response at Kelgraf electrodes*

Voltammetric response obtained for the Kelgraf r.d.e.'s is adequately represented by the i–E curves shown in Fig. 6 for the 3% Kelgraf r.d.e. in the absence (curve a) and presence (curve b) of I^-. The general features of these data are similar to those for the GC r.d.e. (Fig. 3). One exception is that the wave for oxidation of I^- to IO^- is significantly smaller at the 3% Kelgraf r.d.e. Of primary interest to this study is the definite absence of a plateau for IO_3^- production at $E > 1.5$ V. This appears to be a consequence of the positive shift of the $E_{1/2}$ for this anodic wave from the value 1.36 V for the pure GC r.d.e. (Fig. 1) to about 1.47 V for the 3% Kelgraf r.d.e. (Fig. 6). A shift of $E_{1/2}$ is expected for quasi-reversible reactions as the flux density of reactant is increased. Nevertheless, as expected, values of S/B

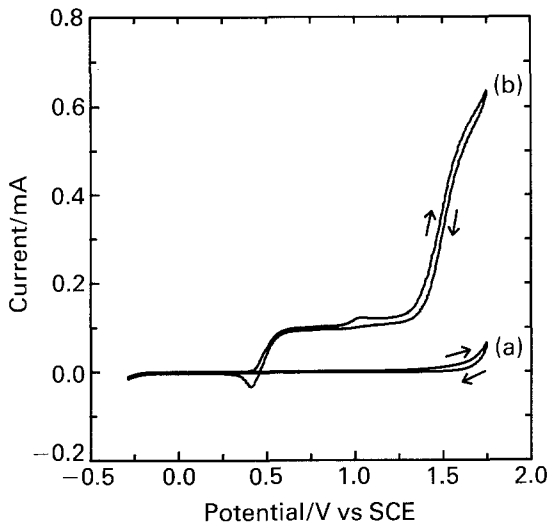

Fig. 6. Voltammetric response (i–E) at a 3% Kelgraf r.d.e. in 0.1 M H_2SO_4 at a scan rate of 100 mV s^{-1}. Rotational velocity: (a) 167.6 and (b) 41.9 s^{-1}. Conc. I^-: (a) 0.0 and 0.50 mM.

are significantly larger at the 3% Kelgraf r.d.e. as compared with the GC r.d.e. This is evident both for iodine production (0.75 V), where the background signal results only from double-layer charging, as well as for IO_3^- production (1.75 V), where oxygen evolution dominates the background signal.

The Levich equation (Equation 5) is not valid for Kelgraf r.d.e.'s since they do not fulfill the requirement of uniform accessibility, i.e. the current density is not equal for all regions of the disc surface. Nevertheless, difference voltammetry has qualitative utility for determination of the dependence of the current response on changes in $\omega^{1/2}$ and C^b, and for extraction of the net transport-dependent i–E response from the total electrode current in regions of the applied potential corresponding to solvent breakdown. Shown in Fig. 7 are values of $\Delta i\{\Delta\omega^{1/2}\}$ (curve a) and $\Delta i\{\Delta C^b\}$ (curve b) plotted against E for the 3% Kelgraf r.d.e. The limiting value of $\Delta i\{\Delta C^b\}$ shown for oxidation of I^- to I_2 is equal to the plateau current measured for 0.5 mM I^-. This indicates that i is a linear function of C^b. In contrast, $\Delta i\{\Delta\omega^{1/2}\}$ is significantly smaller than $\Delta i\{\Delta C^b\}$ for all three anodic processes. This observation is consistent with previous results [24] demonstrating that the $\omega^{1/2}$-dependent response at Kelgraf electrodes decreases as the fractional active area is decreased. Furthermore, it is expected that $\Delta i\{\Delta\omega^{1/2}\}$ approaches zero as the surfaces of composite electrodes approach that of ideal microarray electrodes, i.e. as the fractional active area is decreased.

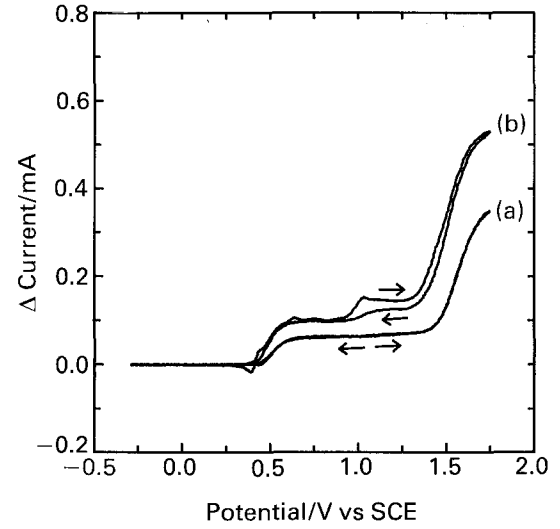

Fig. 7. Difference voltammetric response for I^- at a 3% Kelgraf r.d.e. Curves: (a) $\Delta i\{\Delta\omega^{1/2}\}$–$E$, conditions as in Fig. 2; (b) $\Delta i\{\Delta C^b\}$–E, conditions as in Fig. 3.

As observed above, a detrimental characteristic of the voltammetric response at Kelgraf r.d.e.'s is the positive shift observed for $E_{1/2}$ as the fractional active area is decreased. For oxidation of I^- to IO_3^-, $E_{1/2}$ measured from $\Delta i\{\Delta C^b\}$–E data for $\omega^{1/2} = 6.47\ s^{-1/2}$ increased from 1.34 V at 40% Kelgraf to 1.44 V at 3% Kelgraf in a nearly linear correspondence with decreasing fractional active area. The shift in $E_{1/2}$ was less severe when measured from $\Delta i\{\Delta\omega^{1/2}\}$–$E$ data for 0.50 mM I^-, i.e. 1.49 V at 40% Kelgraf and 1.54 V at 3% Kelgraf. In general, the shift in $E_{1/2}$ for microarray electrodes is caused by an exaggeration of the effect of slow heterogeneous kinetics as a consequence of the enhanced flux density at the active areas.

3.4. *Anodic evolution of oxygen*

Plots of ln $\{i\}$ against E–$E^{0\prime}$ (Equation 4) corresponding to the oxygen-evolution region were used to obtain the product αn for this reaction at each electrode. From the plots for eleven Kelgraf electrodes, the average αn is 0.43 eq mol^{-1} (std. dev. = 0.05) which is in good agreement with the value αn = 0.39 eq mol^{-1} measured for the pure GC electrode. This agreement is interpreted to indicate that the oxygen-evolution mechanisms at GC and the graphitic regions of Kelgraf electrodes are virtually the same.

The current densities (i/A_{act}) measured for oxygen evolution at 1.75 V were slightly larger at Kelgraf than at GC. An average value of 1.83 mA cm^{-2} was measured for the Kelgraf electrodes containing <10% graphite, whereas a value of 1.43 mA cm^{-2} was measured at the GC electrode. The larger values at Kelgraf were probably due to the greater surface roughness and porosity that are characteristic of the composite electrodes. The current density for oxygen evolution increased dramatically for Kelgraf electrodes with >10% graphite content, which is consistent with the dramatic increase in surface roughness caused by the pitting evident in the SEM data for these electrodes.

3.5. *Enhancement of signal-to-background current density*

The relative current density (J), as defined by Equation 6 where A_{act} is the net active electrode

area, has been used to evaluate Kel-F composite electrodes [24].

$$J = \frac{(i/A_{act})_{array}}{(i/A_{act})_{solid}} = \frac{\rho}{1-\theta} \quad (6)$$

In Equation 6, $\rho = (i/A_{geo})_{array}/(i/A_{geo})_{solid}$ where A_{geo} is the geometric electrode area and θ is the inactive fraction of the electrode area. Thus, $A_{act} = (1-\theta)A_{geo}$. Values of ρ and $1-\theta$ vary between 0 and 1, but ρ is always $> 1-\theta$, which results in a significant enhancement in the current density at Kelgraf composite electrodes. However, the value of J is equal to the enhancement in S/B only when the background current is directly proportional to the active electrode area. Here, S/B values were measured as a function of fractional active area and are compared to the J values for the same electrodes.

Values of difference signal ($S = \Delta i\{\Delta C^b\}$ and $\Delta i\{\Delta\omega^{1/2}\}$), measured at 1.75 V, were normalized with respect to the background current ($B = i_{bkd}$), also measured at 1.75 V, to give the observed S/B values for each electrode. These values are listed in Table 1 along with the respective values of J. Also given are S/B values normalized by S/B for the solid GC r.d.e. It is to be expected in Table 1 that a large disparity will exist between values of J and S/B calculated from $\Delta i\{\Delta C^b\}$ and from $\Delta i\{\Delta\omega^{1/2}\}$ data. This disparity results because $\Delta i\{\Delta\omega^{1/2}\} \to 0$ for electrode surfaces approaching the ideal for microarray electrodes. Nevertheless, results based on both sets of data are included for the purpose of comparison.

Values of J and normalized values of S/B are expected to be equal only for the experimental situation where the background current is directly proportional to the projected materials as compared to the solid electrode. As is apparent in Table 1 for the Kelgraf electrodes, the normalized values of S/B are generally much smaller than values of J. This is especially severe for Kelgraf electrodes with greater than 20% graphite, for which the high degree of surface roughness and porosity results in normalized S/B values less than one. This indicates that current efficiencies for oxidation of I^- to IO_3^- at these composite electrodes are smaller than for the GC electrode.

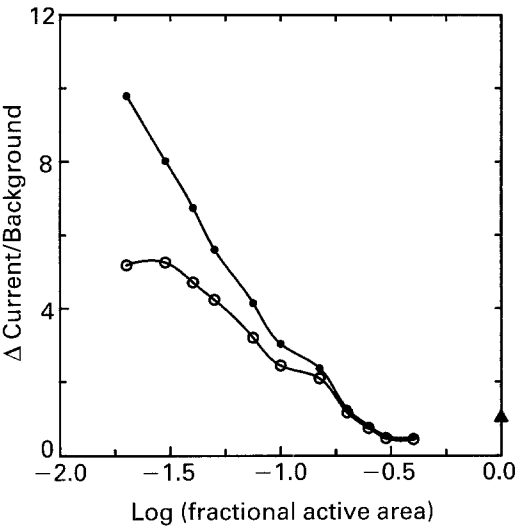

Fig. 8. Difference current (●, $\Delta i\{\Delta C^b\}$; ○, $\Delta i\{\Delta\omega^{1/2}\}$) for the oxidation of I^- to IO_3^- normalized with respect to the background (i_{bkd}) from oxygen evolution at 1.75 V as a function of fractional active area. Values of $\Delta i\{\Delta C^b\}$ and $\Delta i\{\Delta\omega^{1/2}\}$ for the solid GC r.d.e. (▲) are included for comparison.

Values of S/B are plotted in Fig. 8 as a function of the fractional active area of the Kelgraf composites. The values for the GC r.d.e. ($A_{act}/A_{geo} = 1$) are also shown for comparison. At high fractional active areas ($> \sim 15\%$), the values calculated from $\Delta i\{\Delta\omega^{1/2}\}$ are equal to those calculated from $\Delta i\{\Delta C^b\}$, indicating the current is limited by convective-diffusional mass transport. However, as expected for low fractional active areas ($< \sim 20\%$ Kelgraf), the values of S/B calculated from $\Delta i\{\Delta\omega^{1/2}\}$ are substantially smaller than those calculated from $\Delta i\{\Delta C^b\}$. In fact, when the fractional active area is $< \sim 5\%$, S/B calculated from $\Delta i\{\Delta\omega^{1/2}\}$ no longer increases as the fractional active area was decreased. This effect is caused by the decreased dependence of current on $\omega^{1/2}$ as the

*Table 1. Values of S/B corresponding to difference voltammetric signals for IO_3^- production divided by the background current for oxygen evolution and comparison to the relative current density (J) at various Kelgraf electrodes and glassy carbon**

Electrode	$S/B = \Delta i\{\Delta C^b\}/i_{bkd}$		$J\{\Delta C^b\}$	$S/B = \Delta i\{\Delta\omega^{1/2}\}/i_{bkd}$		$J\{\Delta\omega^{1/2}\}$
	Observed	*Normalized*†	*Observed*	*Observed*	*Normalized*†	*Observed*
Glassy carbon	1.09	1.00	1.00	1.10	1.00	1.00
40% Kelgraf	0.51	0.47	1.76	0.44	0.40	1.51
30% Kelgraf	0.54	0.50	2.71	0.47	0.43	2.38
25% Kelgraf	0.81	0.74	2.81	0.74	0.67	2.56
20% Kelgraf	1.26	1.16	3.68	1.17	1.06	3.37
15% Kelgraf	2.36	2.17	4.46	2.09	1.90	3.92
10% Kelgraf	3.03	2.78	5.25	2.44	2.22	4.20
7.5% Kelgraf	4.14	3.80	5.24	3.20	2.91	4.02
5% Kelgraf	5.61	5.15	7.56	4.24	3.85	5.67
4% Kelgraf	6.74	6.18	8.52	4.71	4.28	5.92
3% Kelgraf	8.02	7.36	8.49	5.26	4.78	5.53
2% Kelgraf	9.79	8.98	8.96	5.18	4.71	4.71

* $\Delta i\{\Delta C^b\}$ obtained for $\omega^{1/2} = 6.47\,s^{-1/2}$ with $\Delta C^b = 0.50$ mM.
$\Delta i\{\Delta\omega^{1/2}\}$ obtained for 0.5 mM with $\Delta\omega^{1/2} = 6.47\,s^{-1/2}$.
† These values are normalized with respect to $\Delta i/i_{bkd}$ for the solid GC r.d.e. to allow comparison to J values.

microelectrodes become smaller and more widely spaced.

4. Conclusions

Values of signal-to-background ratio (S/B) for electrochemical processes at hydrodynamic electrodes with nonuniformly active surfaces are more accurately calculated from voltammetric data obtained as a function of change in bulk concentration of the electroactive species rather than changes in rotational velocity. Accordingly, values of S/B for oxidation of I^- to IO_3^- at 1.75 V in 0.1 M H_2SO_4 were determined to be as much as nine times larger for a 2% Kelgraf r.d.e. as compared to a solid GC r.d.e. This can be explained on the basis of (i) the significant decrease in total background current as a result of the decreased fraction of the Kelgraf surface that corresponds to carbon, and (ii) the larger flux density of I^- at the existing carbon microelectrodes in the Kelgraf r.d.e., as compared to the GC r.d.e., as a result of radial diffusion, i.e. the so-called 'edge effect'. A consequence of this enhancement in S/B is an increased current efficiency ($S/(S+B)$) for IO_3^- production from 52% at the solid GC r.d.e. to 91% at the 2% Kelgraf r.d.e. in spite of the simultaneous anodic discharge of H_2O with some evolution of oxygen.

This enhancement in current efficiency was obtained in spite of two detrimental voltammetric characteristics observed for Kelgraf: (i) the $E_{1/2}$ value for IO_3^- production was observed to be shifted to more positive potentials as a result of a greater effect of slow heterogeneous kinetics as a consequence of the higher flux density of I^-; and (ii) the background current for anodic evolution of oxygen was larger than expected because the roughness of the Kelgraf surfaces was greater than that of the solid GC surface. Fabrication of microelectrode arrays with surface roughness equal to that of their solid counterparts could lead to an even greater enhancement in current efficiency for anodic reactions which occur concurrently with oxygen evolution. However, for reactions having especially slow heterogeneous kinetics, the positive shift in $E_{1/2}$ values might decrease or even eliminate the observed improvements in S/B and $S/(S+B)$.

Iodate is a strong oxidizing agent in acidic media ($E^0 = 1.085$ V vs SHE) and the electrochemical production of IO_3^- at high current efficiency might be useful for indirect oxidation of some organic compounds. However, the greater significance of this work is the indication that microelectrode arrays can have more general utility than solid electrodes for electrosynthesis when large potentials are applied that can result in solvent breakdown.

Acknowledgements

We are grateful to Mary Simpson and the 3M Co. for the donation of Kel-F-81 powder. We also acknowledge Warren Straszheim of Ames Laboratory for the SEM data. Ames Laboratory is operated for the US Department of Energy by Iowa State University under Contract W-7405-ENG-82. This publication was supported by the Office of Basic Energy Sciences.

References

[1] J. P. Hoare, 'The Electrochemistry of Oxygen', John Wiley and Sons, New York (1968) p. 86.
[2] J. O'M. Bockris, *J. Chem. Phys.* **24** (1956) 817.
[3] S. Trasatti, *J. Electroanal. Chem.* **111** (1980) 125.
[4] P. Ruetschi and P. Delahay, *J. Chem. Phys.* **23** (1955) 556.
[5] J. E. Vitt and D. C. Johnson, *J. Electrochem. Soc.* **139** (1992) 774.
[6] T. D. Cabelka, D. S. Austin and D. C. Johnson, *ibid.* **131** (1984) 1595.
[7] D.S. Austin, D. C. Johnson, T. G. Hines and E. T. Berti, *Anal. Chem.* **55** (1983) 2222.
[8] I.-H. Yeo, S. Kim, R. Jacobson and D. C. Johnson, *J. Electrochem. Soc.* **136** (1989) 1395.
[9] W. R. LaCourse, Y.-L. Hsiao, D. C. Johnson and W. H. Weber, *ibid.* **136** (1989) 3714.
[10] H. Chang and D. C. Johnson, *ibid.* **137** (1990) 2452.
[11] H. Chang and D. C. Johnson, *ibid.* **136** (1989) 17.
[12] S. Pons and M. Fleischmann, *Anal. Chem.* **59** (1987) 1391A.
[13] R. M. Wightman and D. O. Wipf, 'Electroanalytical Chemistry', Vol. 15, (edited by A. J. Bard), Marcel Dekker, New York (1989) pp. 267–353.
[14] D. E. Tallman and S. L. Petersen, *Electroanal.* **2** (1990) 499.
[15] D. E. Weisshaar and D. E. Tallman, *Anal. Chem.* **55** (1983) 1146.
[16] J. E. Anderson, D. E. Tallman, D. J. Chesney and J. L. Anderson, *ibid.* **50** (1978) 1051.
[17] J. E. Anderson, J. B. Montgomery and R. Yee, *ibid.* **63** (1991) 653.
[18] J. L. Anderson and D. J. Chesney, *ibid.* **52** (1980) 2156.
[19] D. J. Chesney, J. L. Anderson, D. E. Weisshaar and D. E. Tallman, *Anal. Chim. Acta* **124** (1981) 321.
[20] D. E. Weisshaar, D. E. Tallman and J. L. Anderson, *Anal. Chem.* **53** (1981) 1809.
[21] D. E. Tallman and D. E. Weisshaar, *J. Liq. Chromatogr.* **6** (1983) 2157.
[22] J. L. Anderson, K. K. Whiten, J. D. Brewster, T-Y. Ou and W. K. Nonidez, *Anal. Chem.* **57** (1985) 1366.
[23] T-Y. Ou and J. L. Anderson, *ibid.* **63** (1991) 1651.
[24] J. E. Vitt, D. C. Johnson and D. E. Tallman, *ibid.* **65** (1993) 231.
[25] V. G. Levich, 'Physicochemical Hydrodynamics', Prentice Hall, Englewood Cliffs, NJ (1962) p. 75.
[26] R. Mills and V. M. M. Lobo, 'Self-Diffusion in Electrolyte Solutions', Elsevier, New York (1989) p. 318.
[27] G. Milazzo and S. Caroli, 'Tables of Standard Electrode Potentials', John Wiley & Sons, New York (1978).